# Geometry and external field positionally controlled nematic topological defects

Pavlo Kurioz<sup>1</sup>, Marko Kralj<sup>2</sup>, Bryce S. Murray<sup>3</sup>, Charles Rosenblatt<sup>3</sup>, and Samo Kralj\*<sup>4,5</sup>

Address: <sup>1</sup>Jozef Stefan International Postgraduate School, Jamova 39 , 1000 Ljubljana, Slovenia

<sup>2</sup>Comtron, Trzaska 21, 2000 Maribor, Slovenia

<sup>3</sup>Department of Physics, Case Western Reserve University, Cleveland, Ohio 44106-7079, USA

<sup>4</sup>Department of Physics, Faculty of Natural Sciences and Mathematics, University of Maribor, Koroska cesta 160, 2000 Maribor, Slovenia

<sup>5</sup>Jozef Stefan Institute, Jamova 39, 1000 Ljubljana, Slovenia

samo.kralj@um.si

\* Corresponding author

#### **Abstract**

Using a Landau—de Gennes approach, we study the impact of confinement topology, geometry and external fields on spatial positioning of nematic topological defects (TDs). In quasi two-dimensional systems we demonstrate that confinement enforced total topological charge m>>1 decays into *elementary* TDs bearing charge *m*=1/2. These assemble close to the bounding substrate to enable essentially bulk-like uniform nematic ordering in the central part of a system. This effect is reminiscent of the Faraday cavity phenomenon in electrostatics. We observe that in certain confinement geometries, varying the order parameter correlation length size could trigger global rotation of an assembly of TDs. Finally, we show that an external electric field could be used to drag the boojum finger tip towards a confinement cell interior. Assemblies of TDs could be exploited as traps for appropriate nanoparticles, opening several opportunities for development of functional nanodevices.

# **Keywords**

Topological defects; nematic liquid crystals; topological charge; nanoparticles

#### Introduction

Topological defects (TDs) [1] represent an interdisciplinary research area [2] which is of high interest for nearly all branches of science. Due to their topological origin they exhibit several universal features that are independent of system's microscopic details in which TDs appear. Their complete understanding might even resolve some of the most intriguing unanswered questions of nature. Namely, there are several strong indications that *fields* represent basic entities of nature and not *fundamental particles* [3] - which are in this case emergent phenomenon. For example, as far back as 1962 Skyrme [4] developed a theory in which he described hadrons as topological defects in the *pion field*.

A convenient system in which to study fundamental behaviour of TDs are various liquid crystal (LC) phases [5]. They are relatively easily accessible to various experimental methods [6] due to their unique combination of optical anisotropy and transparency, fluid character, and mechanical softness. In addition, the diversity of LC phases and structures guarantees the existence of many qualitatively different TD structures.

Several recent studies reveal that TDs in LCs could efficiently positionally control assemblies of appropriate nanoparticles (NPs) [7,8,9]. Note that order parameters, which can host defects, possess two qualitatively different components [10]: an amplitude (also referred to as a hydrodynamic) field, and a symmetry breaking (also referred to as a gauge or nonhydrodynamic) field. If a nanoparticle's characteristic size is comparable to an order parameter's amplitude correlation length (which roughly estimates the core size of a defect), and if the nanoparticle does not

sufficiently disturb the symmetry breaking field surrounding the defect's core, then the defect could efficiently trap the NP due to the Defect Core Displacement (DCR) mechanism [11]. Namely, in this case a relatively energetically expensive defect core volume is (at least partially) replaced by NP's volume, thereby reducing the overall energy. It has been shown that lattices of orientational (disclinations) [11,12] and translational (dislocations) [9] defects can readily trap such NPs. Furthermore, it was demonstrated that line defects could be exploited to form nanowire-type structures [9,13] consisting of NPs.

In this contribution we study numerically the effects of geometry and an external electric field on positions of nematic TDs using the Landau-de Gennes mesoscopic approach.

# Theoretical Background

Of interest is the impact of confinement and/or an external electric field on topological defects in a nematic liquid crystal. We use the Landau-de Gennes approach [5] in terms of the tensor order parameter Q. In its eigenframe it is expressed as

 $\underline{Q} = \sum_{i=1}^{3} \lambda_{i} \vec{e}_{i} \otimes \vec{e}_{i}$ , where  $\vec{e}_{i}$  and  $\lambda_{i}$  correspond to corresponding eigenvectors and eigenvalues, respectively. We consider uniaxial LCs where the bulk equilibrium ordering is described by the uniaxial tensor

$$\underline{Q} = S\left(\vec{n} \otimes \vec{n} - \frac{1}{3}\underline{I}\right),\tag{1}$$

The unit vector  $\vec{n}$  points along the local uniaxial direction and is referred to as the nematic director, the uniaxial orientational order parameter S quantifies the extent of fluctuations about  $\vec{n}$ , and I is the unit tensor. If the LC ordering is distorted, the

system could exhibit biaxial states. In simulations we study topological defects either in the Cartesian coordinate system (x,y,z) or in the cylindrical coordinate system  $(r,\varphi,z)$ . Their coordinate frames are determined by the unit vectors  $(\vec{e}_x,\vec{e}_y,\vec{e}_z)$  and  $(\vec{e}_r,\vec{e}_\varphi,\vec{e}_z)$ , respectively. We parameterize the nematic order parameter as

$$\underline{Q} = (q_3 + q_1)\vec{e}_x \otimes \vec{e}_x + (q_3 - q_1)\vec{e}_y \otimes \vec{e}_y + q_2(\vec{e}_x \otimes \vec{e}_y + \vec{e}_y \otimes \vec{e}_x) - 2q_3\vec{e}_z \otimes \vec{e}_z,$$
(2)

$$\underline{Q} = (q_3 + q_1)\vec{e}_r \otimes \vec{e}_r + (q_3 - q_1)\vec{e}_z \otimes \vec{e}_z + q_2(\vec{e}_r \otimes \vec{e}_z + \vec{e}_z \otimes \vec{e}_r) - 2q_3\vec{e}_\omega \otimes \vec{e}_\omega,$$
(3)

where  $\{q_1, q_2, q_3\}$  are the variational parameters.

A convenient metric or the degree of biaxiality is the biaxiality parameter [14,15]

$$\beta^2 = 1 - \frac{6\left(tr\underline{Q}^3\right)^2}{\left(tr\underline{Q}^2\right)^3} \in [0,1]. \tag{4}$$

A uniaxial state and maximal biaxiality configurations are signaled by  $\beta^2 = 0$  and  $\beta^2 = 1$ , respectively.

#### Free energy and scaling

We write the free energy as the sum of volume and surface integrals

$$F = \iiint (f_c + f_e + f_f) d^3 \vec{r} + \iint f_s d^2 \vec{r}$$
. The condensation  $(f_c)$ , elastic  $(f_e)$  and external

electric field  $(f_f)$  free energy densities are expressed as [5,15]

$$f_c = \frac{A_0(T - T^*)}{2} tr \underline{Q}^2 - \frac{B}{3} tr \underline{Q}^3 + \frac{C}{4} \left( tr \underline{Q}^2 \right)^2, \tag{5}$$

$$f_{\rm e} = -\frac{L}{2} \left| \nabla \underline{\mathbf{Q}} \right|^2,\tag{6}$$

$$f_{t} = -\frac{1}{2}\varepsilon_{0}\Delta\varepsilon\vec{E}\cdot\vec{Q}\vec{E},\tag{7}$$

respectively. The quantities  $A_0$ , B, C are material constants,  $T^*$  is the supercooling temperature, L is representative characteristic elastic constant in the single elastic

constant approximation,  $\vec{E}$  is an external electric field,  $\varepsilon_0$  is the permittivity of free space, and  $\Delta\varepsilon$  is the dielectric constant anisotropy. We model conditions at the LC confining boundaries either by [15,16]

$$f_s = \frac{W}{2}\vec{\mathbf{v}} \cdot \underline{\mathbf{Q}}\vec{\mathbf{v}},\tag{8}$$

or

$$f_{\rm s} = \frac{w}{2} tr \left( \underline{Q} - \underline{Q}_{\rm s} \right)^2, \tag{9}$$

where w is the surface interaction strength,  $\vec{v}$  is the local confinement surface normal, and  $\underline{Q}_s$  describes surface preferred nematic ordering. The surface term given by Eq.(8) enforces for w>0 (w<0) degenerate tangential (homeotropic) anchoring. On the other hand, the contribution in Eq.(9) is minimized for  $\underline{Q} = \underline{Q}_s$ , assuming w>0. In simulations we consider cases where  $\underline{Q}_s$  enforces uniaxial ordering given by Eq.(1), where S possesses the bulk equilibrium value, and [5,17]

$$\vec{n} = \vec{e}_x \cos \theta + \vec{e}_y \sin \theta, \quad \theta = m \tan^{-1}(y / x).$$
 (10)

This ansatz enforces topological defect of strength m, where m is an integer multiple of  $\frac{1}{2}$ .

For numerical and presentational convenience [15], we introduce the reduced temperature  $\tau = \frac{24A_0(T-T^*)}{B^2} = \frac{T-T^*}{T^{**}-T^*}$ , where  $T^{**}$  is the nematic superheating temperature. In this scaling the bulk phase transition temperature  $T_{IN}$  corresponds to  $\tau_{IN} = \frac{T_{IN}-T^*}{T^{**}-T^*} = \frac{8}{9}, \text{ and the bulk degree of uniaxial ordering minimizing Eq.(5) can be expressed as } S_{eq}(\tau \le \tau_{IN}) = S_0(1+\sqrt{1-\tau}), \ S_0 = S_{eq}(T^{**}) = B/(4C).$ 

LC material properties are reflected in various characteristic lengths describing responses of LC ordering to different perturbations. The relevant lengths for our study are the biaxial correlation length  $\xi_b$ , the external field coherence length  $\xi_E$ , and the surface extrapolation length  $d_{\rm e}$ . We define them as

$$\xi_{b} = \sqrt{\frac{4LC}{B^{2}\left(\sqrt{1-\tau}+1\right)}}, \quad \xi_{E} = \sqrt{\frac{LS_{0}}{\varepsilon_{0}\left|\Delta\varepsilon\right|E^{2}}}, \quad d_{e} = LS_{0} / w. \tag{11}$$

Note that for scaling purposes we expressed the latter two distances at  $T = T^{**}$ .

To estimate their values we choose material properties of typical nematic LC. As a representative we took 5CB, for which [5]  $A_0 \sim 0.3 \, 10^6$  J/(Km³),  $B \sim 4.8 \, 10^6$  J/m³,  $C \sim 1.6 \, 10^7$  J/m³,  $L \sim 10^{-11}$  J/m,  $\Delta \varepsilon \sim 5$ ,  $T_{IN} \sim 318$  K,  $T_{IN} = T^* \sim 1.1$  K,  $T^{**} = T_{IN} \sim 0.18$ . For temperatures close below  $T_{IN}$  it follows  $\xi_b \sim 20$  nm,  $\xi_E(E \sim 10^6 \text{ V/m}) \sim 1 \, \mu\text{m}$ ,  $d_e(w \sim 10^{-4} \text{ J/m}^2) \sim 1 \, \mu\text{m}$ .

We obtained nematic structures for given boundary conditions by minimizing the total free energy of the system. The resulting Euler-Lagrange equilibrium equations for the variational parameters {  $q_1$ ,  $q_2$ ,  $q_3$ } are solved using the standard over-relaxation method, where the calculation details are given in [15].

#### Geometry of the problem

We consider thin plane-parallel cells of thickness h. The top and bottom plates are placed at z=0 and z=h, respectively. We consider the cells either in the Cartesian (x,y,z) or cylindrical geometry  $(r,\varphi,z)$ , as illustrated in Figure 1. Accordingly we use two different boundary conditions, to which we refer as *Boundary Anchoring Condition* (BAC) [18] and *Surface Anchoring Condition* (SAC), respectively.

We use BAC in the "Cartesian" cells. We assume that the cells are relatively thin and the nematic ordering is entirely dominated by conditions at the top "master" plate. At the master plate we impose a strong uniaxial boundary condition of order parameter  $\underline{Q}_s$  qiven by Eq.(10). The latter is either a circle of radius  $R = \sqrt{x^2 + y^2}$  or a trapezoid which we characterized by a distance R. It is assumed that R is large with respect to the relevant nematic order correlation length. Inside the boundary we allow the nematic tensor frame to freely rotate in the (x,y) plane. In these simulations the nematic ordering is effectively two dimensional. Hence, we neglect variations along the z-axis and set Q = Q(x,y).

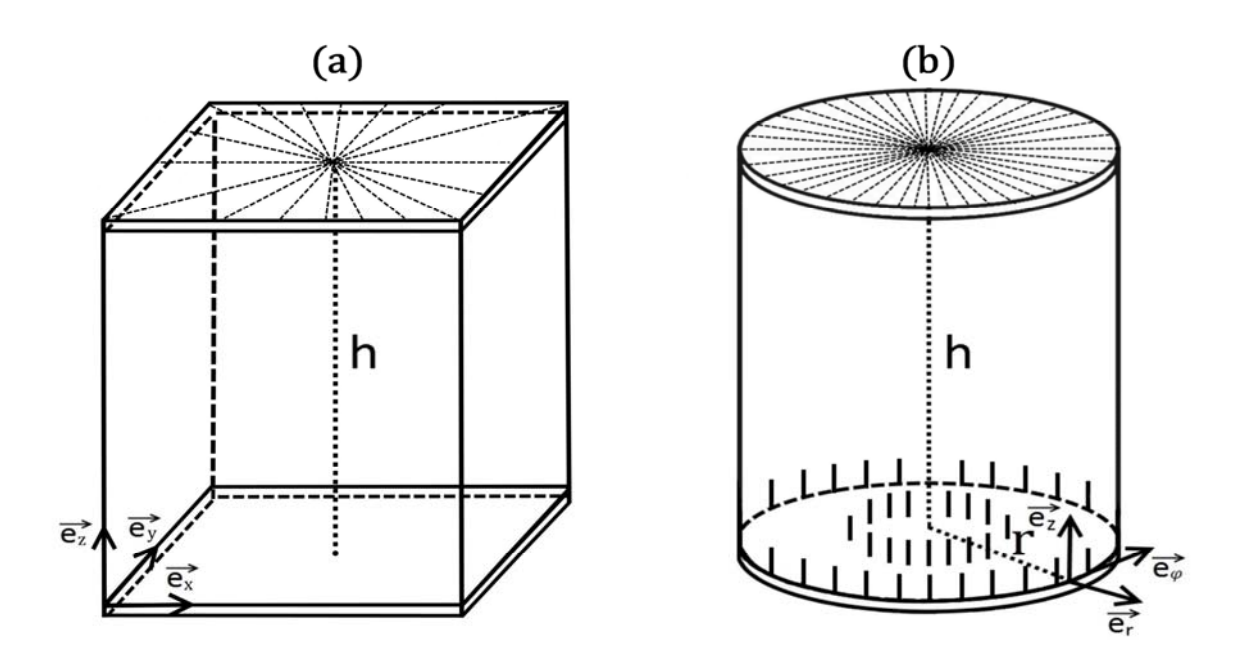


**Figure 1:** Geometry of cells used in simulations. (a) In the "Cartesian" cells we enforce at the top "master" plate uniaxial nematic structures defined by Eq.(10) and assume  $\underline{Q} = \underline{Q}(x,y)$ . (b) In the "cylindrical" cells we impose a boojum topological defect at the top plate and assume  $\underline{Q} = \underline{Q}(r,z)$ .

In the SAC case we consider thicker cells and permit spatial variations along the z direction. For this case we perform simulations in the cylindrical coordinate system [20] and we impose the cylindrical symmetry (i.e., Q = Q(r,z)). At the top plate we enforce uniaxial boundary conditions  $Q_s$  qiven by Eq.(10), in which we set m=1. At the bottom plate we enforce homeotropic anchoring conditions using the ansatz Eq.(8). At the lateral boundaries we assume free boundary conditions. Such conditions impose a boojum topological defect at the top plate [19,20].

Note that in our simulations we mimic geometric set-ups which could be realized experimentally using, for instance, the atomic force microscope (AFM) scribing method [17]. In a typical experimental set up one confines a nematic LC within a thin plane-parallel cell, where at least one ("master") surface imposes anchoring conditions inscribed via an AFM stylus [17,18], with a planar – degenerate "slave" as the other surface. In Figure 2 we depict an example of a "master" substrate enforcing 2D topological defects of strength  $m = \pm 2$ , and corresponding experimentally measured textures using polarized optical microscopy.

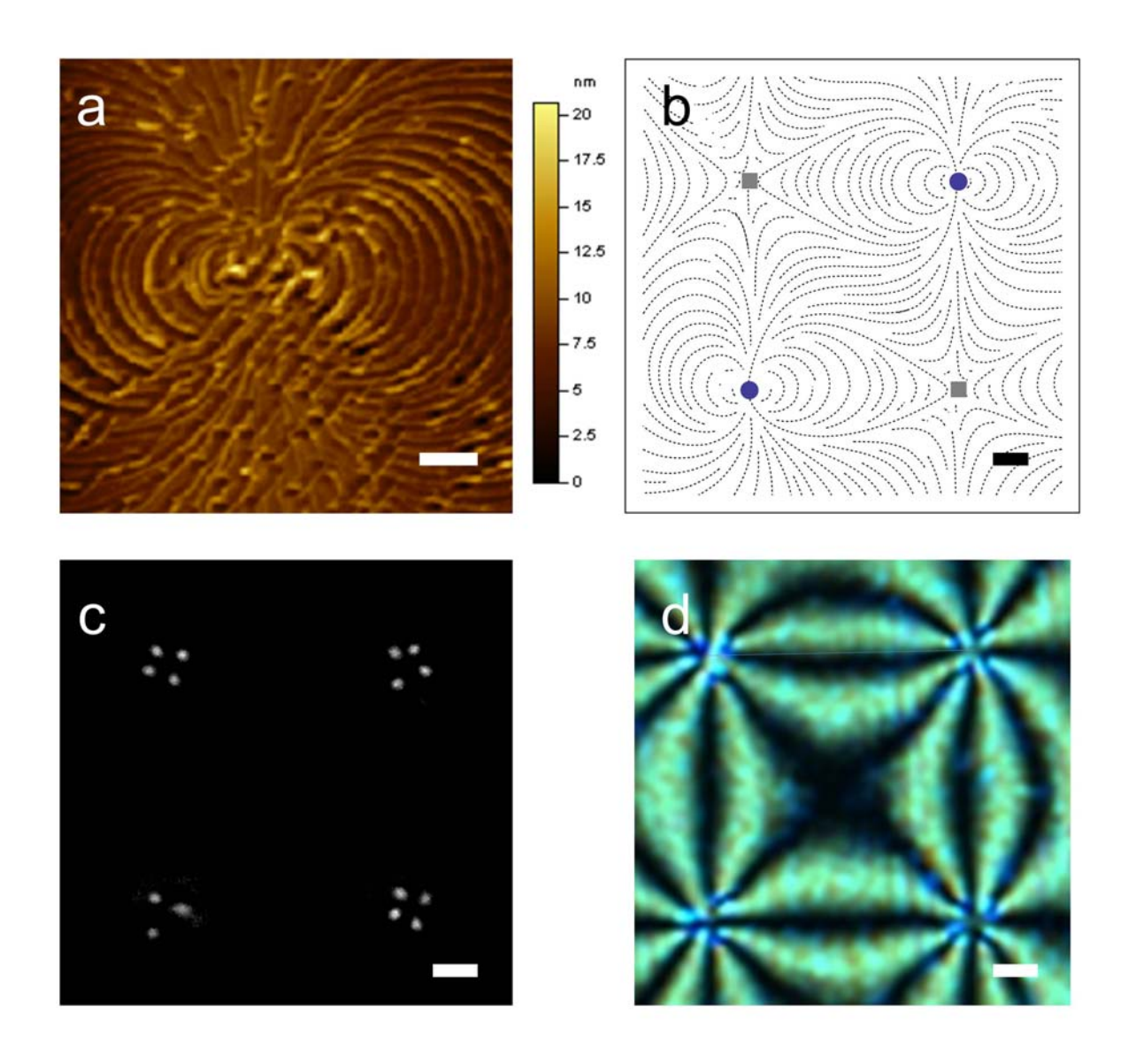


**Figure 2:** Top left: Typical scribed surface topography enforcing the m=2 topological defect. Top right: Schematic representation showing AFM-scribed director pattern of four topological defects (m=2: blue circles, m=-2: gray squares), part of a larger square array of such defects. Separation between nearby defects is roughly 30 μm, h~3 μm. Bottom left: A darkfield microscopy image of a nematic cell whose master plate enforces a square array of m = ±2 TDs; this image shows a rare example of double integer defect that decomposes into a pair of half integer defects plus one integer defect. Bottom right: Typical polarizing microscopy pattern image of this defect array. The scale bars are (a) 500 nm and (b,c,d) 5 μm.

#### **Results and Discussion**

In the following we present results of our simulations. We consider structures using the "Cartesian" cells, where we study how different patterns of TDs emerge.

Afterwards we focus on an external field defect core structure driven changes in the "cylindrical" cell.

#### Faraday cavity effect

We first study patterns emerging from the BAC boundary condition. We enforce the total topological charge of strength m inside the circular boundary of radius R. At the boundary we strongly impose the nematic ordering defined by Eq.(10). The energy-minimized configurations are plotted in Figures 3 and Figures 4.

In Figure 3 we plot equilibrium biaxiality profiles in which cores of TDs are clearly visible. The imposed total charges always decompose into TDs bearing elementary charges  $m_0$ =1/2. The cores of  $m_0$ =1/2 TDs are fingerprinted by a volcano-like rim where  $\beta^2$  =1 [15,18]. For m=1, m=2, m=4 and m=6 the patterns possess 2, 4, 8 and 12 TDs. The TDs tend to assemble close to the boundary. The resulting director orientation is plotted in Figure 4: We plot eigenvectors of  $\underline{Q}$  with the largest positive eigenvalue (which we set to be  $\vec{e}_1$ ), which in the uniaxial limit corresponds to the nematic director field. Note that nematic textures are essentially uniaxial, except close to the defects cores. For this reason we henceforth refer to  $\vec{e}_1$  as the nematic director field. One sees that the ordering becomes increasingly spatially uniform in the central region on increasing m.

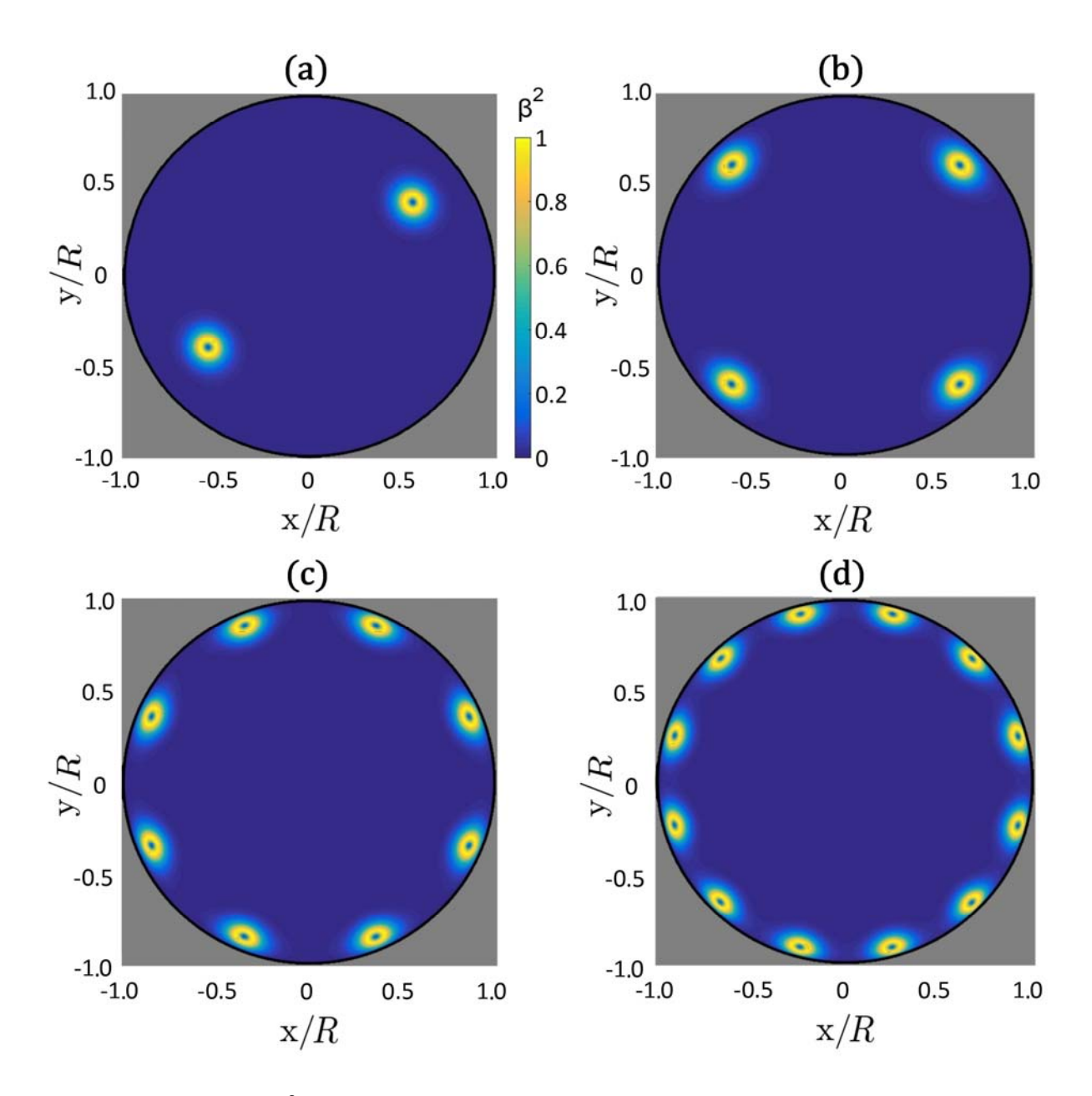


**Figure 3:** Plots of  $\beta^2(x,y)$  for different imposed total topological charges using BAC: (a) m=1, (b) m=2, (c) m=4, (d) m=6. In all cases TDs are decomposed into elementary units bearing the charge  $m_0 = 1/2$ , which assemble close to the bounding circle. In all figures we set  $R/\xi_b = 30$ ,  $\tau = -8$ . The corresponding director field is depicted in Figure 4.

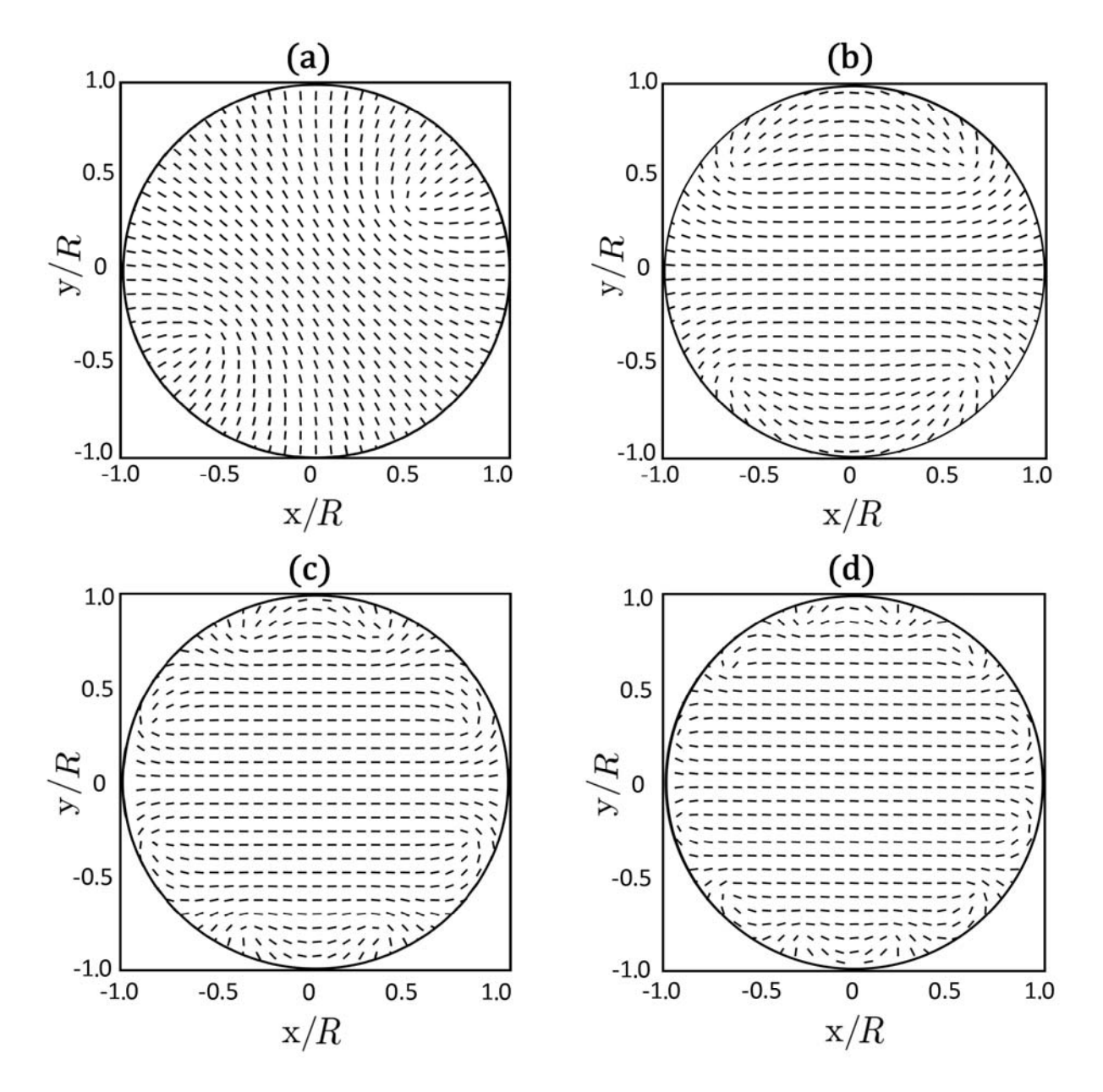


**Figure 4:** 2D Plot of the  $\underline{Q}$  eigenvector with the largest positive eigenvalue, corresponding to the 2D biaxiality profiles  $\beta^2(x,y)$  plotted in Figure 3. (a) m=1, (b) m=2, (c) m=4, (d) m=6.  $R \mid \xi_b = 30$ ,  $\tau = -8$ .

This phenomenon is reminiscent of the Faraday cavity effect in conductors. Namely, if one puts electric charges on a conducting body, the charges assemble at its surface and the resulting electric field inside the body vanishes. The Faraday-like

behavior in our simulations is clearly visible for cases  $R/\xi_b>>1$ . In simulations we set  $R/\xi_b=30$ , and for typical LCs it holds  $\xi_b\sim20\,$  nm.

The absence of an electric field inside the conductor in the electrostatic analogue corresponds in our simulations to a spatially uniform nematic director in the area separated by a distance greater than  $\xi_b$  from the confining boundary.

#### Temperature induced pattern changes

We next consider cases where we change the symmetry of the bounding surface.

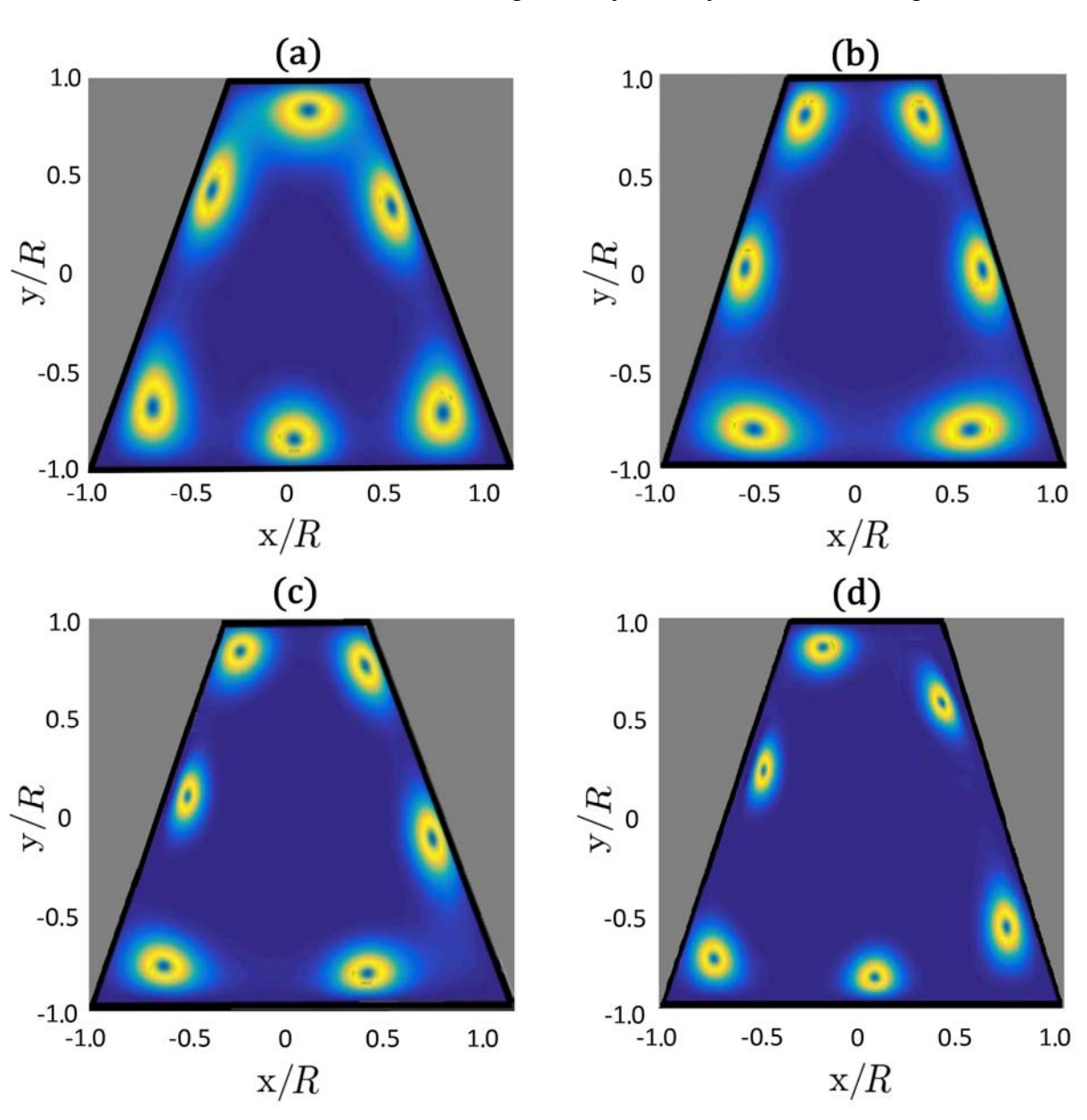


**Figure 5**:  $\beta^2(x,y)$  plots of configuration of TDs on increasing the ratio  $\eta=R/\xi_b$ : (a)  $\eta=14$ , (b)  $\eta=17$ , (c)  $\eta=21$ , (d)  $\eta=25$ . In practice this could be achieved by decreasing temperature of the sample. The trapezoid boundary enforces the total topological charge m=3, which splits into six  $m_0=1/2$  elementary charges.

In Figure 5 and Figure 6 we show nematic configurations for trapezoid shaped boundary, through which we enforce m=3 using Eq.(10). In all cases the imposed charge decays into *elementary* charges  $m_0$ =1/2, and the charges assemble at the confining boundary as discussed in the previous subsection. For this specific confinement symmetry we observe changes in nematic patterns on decreasing the ratio  $\eta = R / \xi_b$ , where R corresponds to the bottom length of the trapezoid.

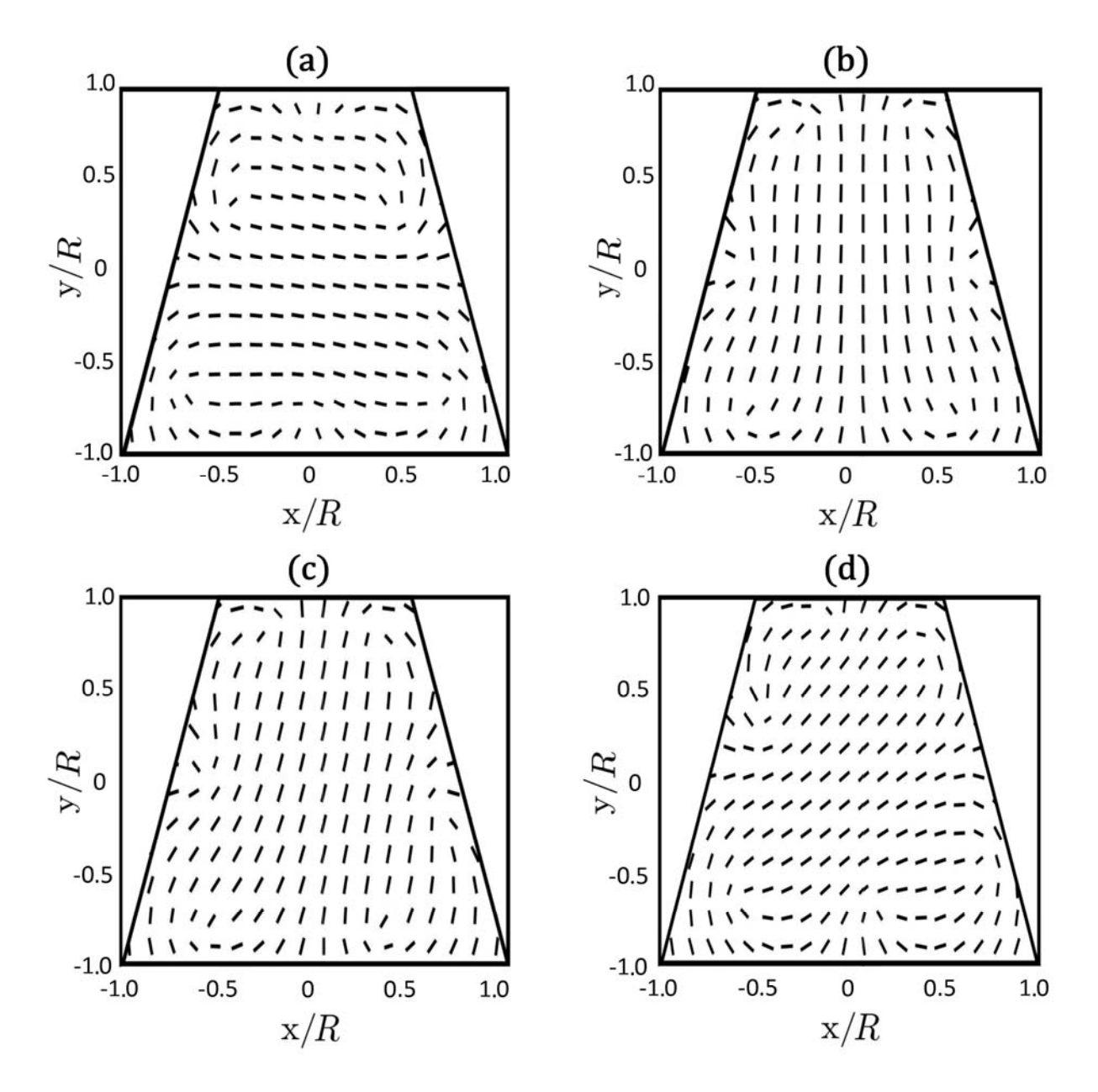


**Figure 6**: Changes in the nematic director field on increasing the ratio  $\eta=R/\xi_b$ : (a)  $\eta=14$ , (b)  $\eta=17$ , (c)  $\eta=21$ , (d)  $\eta=25$ . The corresponding biaxiality profile is depicted in Figure 5.

In practice one could vary  $\eta$  by changing temperature of the sample, which affects  $\xi_b$ . In such case a rotation of defect patterns are expected according to our simulations. The changes in patterns reveal that the system's energy landscape substantially changes on varying  $\eta$ . From the perspective of TDs, the LC

configurations reflect the interplay between mutual repulsion among like defects and interaction of TDs with confinement geometry. Note that for sufficiently symmetric confinement, the "rotation" disappears. It is also sensitive to number of TDs.

#### External field driven boojum tip

We next consider thicker cells and SAC boundary conditions. For sufficiently strong anchoring, a boojum surface defect [19,20] resides at the top surface. Its structure has been studied in detail in [20]. Its surrounding nematic director field resembles a "classical" half-hedgehog structure. On the other hand the core structure is relatively complex [20] and is schematically shown in Figure 7. Its core is characterized by a negatively uniaxial finger, surrounded by a shell exhibiting maximal biaxiality  $\beta^2 = 1$ . The finger-tip is melted due to topological considerations. To understand this let us consider ideal cylindrically symmetry, which we also adopt in our simulations. The symmetry axis of the defect is uniaxial. Namely, in terms of the parametrization defined by Eq.(3) the elastic free energy density includes the term which is linearly proportional with  $\left((3q_1+q_2)^2+q_3^3\right)/r^2$ . The singularity at r=0 can be avoided if uniaxial states are introduced, for which it holds that  $3q_1 + q_2 = q_3 = 0$ . On decreasing z from the top plate, the negative uniaxiality extends to the finger-tip (see Figure 8). Below the tip the axis is positively uniaxial. The transition from negative to positive uniaxiality requires melting of the nematic ordering in the intervening area. A typical director field spatial variation  $\vec{n} \sim \vec{e}_1 = \vec{e}_r \sin \theta + \vec{e}_z \cos \theta$  in the radial direction and order parameter changes along the symmetry axis are depicted in Figure 8. In the case shown the finger tip (where the nematic ordering is melted) is located at  $(r,z) = (0,h-\xi_f)$ , where  $\xi_f \sim 0.8 \xi_b$ . For  $z > h-\xi_f$  the director field is roughly radial

everywhere and S(r=0,z)<0. On the other hand, for  $z < h - \xi_f$  the nematic order is positively uniaxial at r=0 and  $\vec{n} = \vec{e}_z$ . On increasing r the director field monotonically increases its departure from the z-axis.

We next apply an external electric field along the *z*-axis and assume that the LC possesses a negative dielectric anisotropy ( $\Delta\varepsilon$  < 0). It this case the external field favors the negatively uniaxial part of the boojum. Consequently, it becomes elongated on increasing the field strength, as it is illustrated in Figure 9. For this purpose the external field must be relatively strong, *i.e.*,  $\xi_E \sim \xi_b$ , which in a typical LC would correspond to  $E\sim 10^8$  V/m.

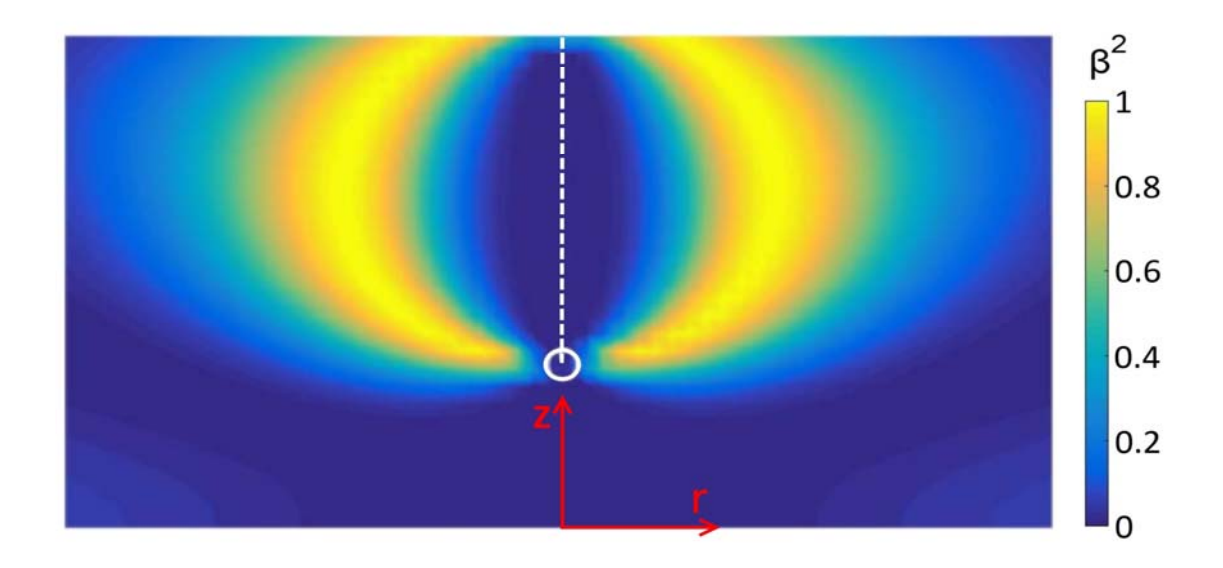


**Figure 7**: Cross-section through a cylindrically symmetric boojum core structure. The biaxial shell exhibiting maximal biaxiality joins the melted finger-tip with the top plate. In the case shown, the anchoring strength at the top plate is finite. The negative uniaxial region is indicated by a dashed white line. The finger-tip is marked with a circle. The bar code determines values of  $\beta^2$ .

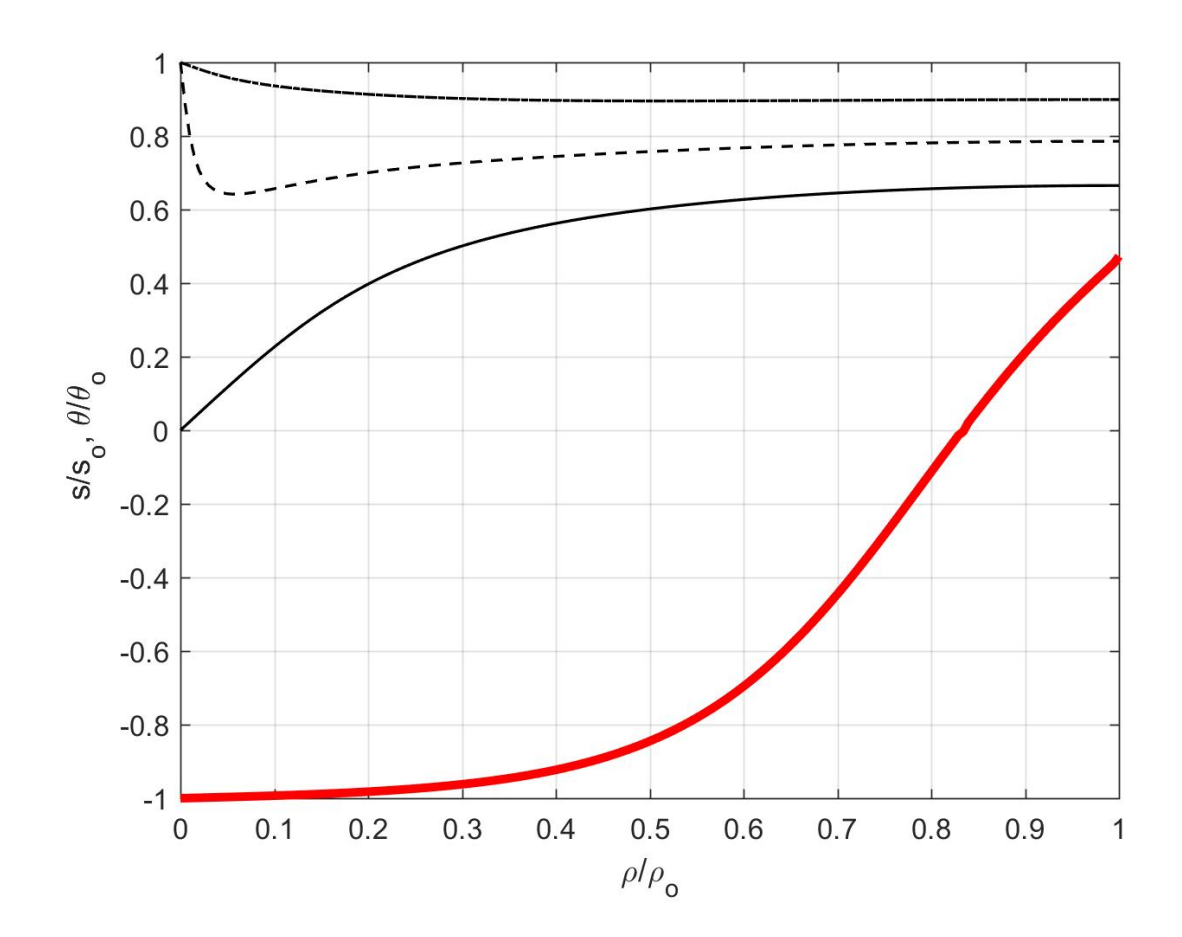


**Figure 8**: Radial spatial variation of the director field (thin black lines,  $\rho \equiv r$ ,  $\rho_0 \equiv \xi_b$ ;  $\theta_0 = \pi/2$ ), and degree of uniaxial order along the symmetry axis (thick red line,  $z \equiv \rho$ ,  $\rho_0 \equiv h$ ;  $S_0 = \left|S(r=0,z=h)\right|$ , r=0). In the simulations we establish a strong anchoring condition at the top plate,  $h/\xi_b = 8$ ,  $\tau = -8$ .

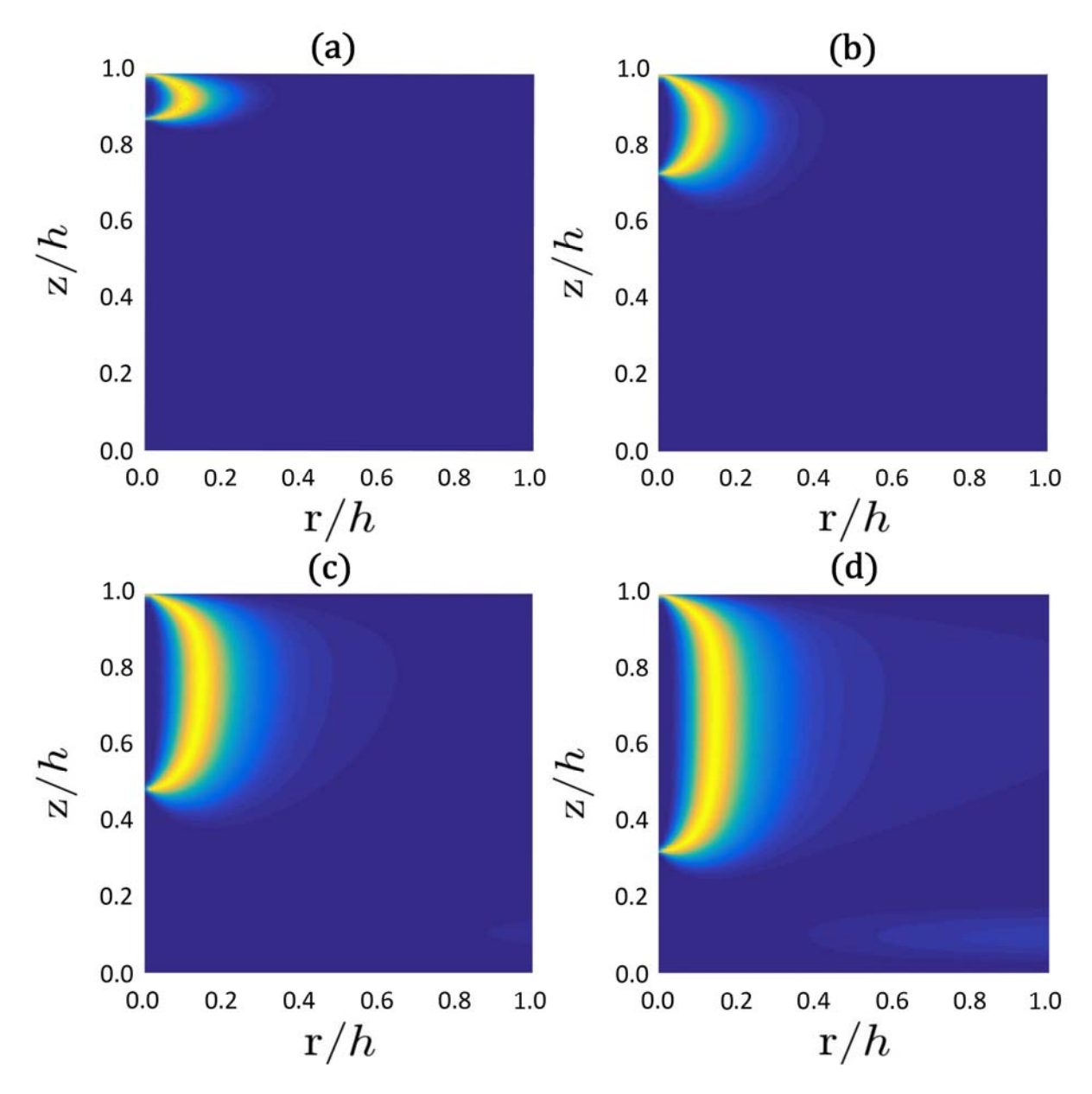


**Figure 9**: Extension of the finger-tip with an increasing external field. Owing to the cylindrical symmetry, we plot only the right-hand part of the boojum core structure (see Figure 8). (a)  $h/\xi_E=0$ , (b)  $h/\xi_E=8$ , (c)  $h/\xi_E=10$ , (d)  $h/\xi_E=12$ .  $h=10\xi_b$ ,  $h/d_e=100$ ,  $\tau=-8$ .

# Conclusion

We studied numerically the impact of geometry, topology, and external field on patterns and position of nematic topological defects. In our phenomenological study we used the Landau – de Gennes approach in terms of the nematic tensor order parameter. We found that, in quasi 2D systems, TDs rearrange relatively close to the bounding line, which topologically enforces their presence. Such assemblies of TDs enable the formation of essentially spatially uniform orientational ordering in the central part of the confined nematic. This effect is reminiscent of the Faraday cavity phenomenon in electrostatics. Furthermore, we demonstrated that, for certain confinement geometries (we chose a trapezoid), one could induce collective rotation of a pattern of TDs on changing the defect core size. For example, the latter could be varied by changing the temperature. Furthermore, we demonstrated that one could extend the boojum finger towards the cell interior if an external field is imposed approximately along its symmetry axis for LCs exhibiting negative external field anisotropy,

These mechanism could be exploited for indirect positional manipulation [7,8,9,11,12] of certain NPs via positionally controlled TDs. Namely, appropriately surface decorated NPs could be efficiently trapped within cores of TDs due to the Defect Core Displacement mechanism. Therefore, by manipulating texture of TDs, one could control the predetermined - or reconfigure the – positions of trapped NPs, which could be exploited in future nano-based devices.

# Acknowledgements

SK acknowledges the financial support from the Slovenian Research Agency (research core funding No. P1-0099). PK acknowledges the Slovenian Human Resources and Scholarship Fund. CR was supported by the National Science Foundation's Condensed Matter Physics program under grant DMR-1505389, and

BSM was supported by the National Aeronautics and Space Administration under grant NNX17AC76G.

### References

- 1. Mermin N.D. Rev. Mod. Phys., 1979, 51, 591-648.
- 2. Zurek, W.H. Nature, 1985, 317, 505-508.
- 3. Hobson, A. Am. J. Phys., 2013, 81, 211-223.
- 4. Skyrme, T.H.R. Nucl. Phys., 1962, 31, 556-569.
- 5. Kleman, M.; Lavrentovich, O.D. *Soft Matter Physics*, **2003**, Springer-Verlag, New York.
- 6. Kurik, M.V.E.; Lavrentovich, O.D. Physics-Uspekhi, 1988, 31, 196-224.
- 7. Kikuchi, H.; Yokota, M.; Hisakado, M.; Yang, H.; Kajiyama, T. *Nat. Mater.* **2002**, *1*, 64-68.
- 8. Karatairi, E.; Rožič, B.; Kutnjak, Z.; Tzitzios, V.; Nounesis, G.; Cordoyiannis, G.; Thoen, J.; Glorieux, C.; Kralj, S., *Phys. Rev. E*, **2010**, *81*, 041703(1)-041703(5).
- 9. Coursault, D.; Grand, J.; Zappone, B.; Ayeb, H.; Levi, G.; Felidj, N.; Lacaze, E. *Adv. Mater.*, **2012**, *24*, 1461-1465.
- 10. Palffy-Muhoray, P.; *Phys. Today*, **2007**, *60*, 54-60.
- 11. Rožič, B.; Tzitzios, V.; Karatairi, E.; Tkalec, U.; Nounesis, G.; Kutnjak, Z.; Cordoyiannis, G.; Rosso, R.; Virga, E.G.; Muševič, I.; Kralj, S. *Eur. Phys. J. E*, **2011**, 34, 17-27.
- 12. Cordoyiannis, G.; Jampani, V. S. R.; Kralj, S.; Dhara, S.; Tzitzios, V.; Basina, G.; Nounesis, G.; Kutnjak, Z.; Tripathi, C. S. P.; Losada-Perez, P.; Jesenek, D.; Glorieux, C.; Musevic, I.; Zidansek, A.; Amenitsch, H.; Thoen, J. *Soft matter*, **2013**, *9*, 3956-3964.

- 13. Ok, J.M.; Kim, Y.H.; Lee, T.Y.; Yoo,H.W.; Kwon, K.; Jung, W.B.; Kim, S.H.; Jung, H.T. *Langmuir*, **2016**, 32, 13418-13426.
- 14. Kaiser, P.; Wiese, W.; Hess, S. J. Non-Equilib. Thermodyn., 1992, 17, 153-169.
- 15. Kralj, S.; Virga, E.G. J. Phys. A: Math. Gen., 2001, 34, 829-838.
- 16. Nobili, M.; Durand, G. Phys. Rev. A, 1992, 46, R6174- R6177.
- 17. Murray, B.S.; Pelcovits, R.A.; Rosenblatt, C. *Phys. Rev. E*, **2014**, *90*, 052501(1) 052501(6).
- 18. Kralj, S.; Murray, B.S.; Rosenblatt, C. *Phys. Rev. E.* 95, **2017**, 042702(1)-042702(9).
- 19. Volovik, G.E. JETP Lett. 1978, 28, 59-62.
- 20. Kralj, S.; Rosso, R.; Virga, E.G. Phys. Rev. E, 2008, 78, 031701(1) 031701(4).